Toward an Integrated Computational Materials Engineering (ICME) Model for D-LFT Process

*Y. Fan[1], Y.C Liu[1], G. Meirson[2], V. Ugresic[2], A. N. Hrymak[3] and J. T. Wood[1]**

[1]Department of Mechanical and Materials Engineering, University of Western, London, Ontario, Canada

[2]Fraunhofer Project Centre for Composites Research University of Western Ontario

[3]Department of Chemical and Biochemical Engineering, University of Western, London, Ontario, Canada

Abstract: Due to the superior properties of polyamide compared to polypropylene, direct compounding of glass fiber reinforced polyamide is currently attracting research interest. These materials are expected to provide both increased modulus, strength and toughness, which can be advantageous for automotive lightweighting endeavours. However, more work is required to achieve insight into the relationship between processing, microstructure and mechanical properties of the prospective long fiber thermoplastic (D-LFT) system. In the present study, direct compounding trials were conducted to study long glass fiber reinforced polyamide 6 compression molded composites. Numerical prediction of fiber orientation was compared with experimental observations. A simulation of plaque manufacturing in a compression molding process was performed. Flow and fiber orientation of PA6 with 30% weight glass was studied using Moldex3D. The effect of initial fiber orientation on the final orientation was studied. It was observed that the walls have a significant effect on fiber orientation and that fiber orientation differs between the skin and the core of the material. Mechanical properties are predicted using established structure-property models and measured microstructural quantities and are compared to experimental values. Results suggest that an integrated computational materials engineering (ICME) model is achievable for the D-LFT process.

Key Words: ICME, D-LFT, fiber orientation, mechanical properties, polyamide 6, glass fiber

1 Introduction

Due to the high performance-to-cost ratio and mass productivity, direct-compound long fiber reinforced thermoplastics (D-LFTs) are attracting more and more attention from the automotive industry [1, 2]. Since the fiber architecture plays a dominant role in determining the mechanical properties of D-LFT materials, fiber length and fiber orientation are intensively investigated [3-5]. During the typical extrusion compression molding (D-LFT-ECM) process, fibers are incorporated into a twin-screw extruder to be compounded with the melt polymers. The specially designed cutting element of the screws gives the fibers a typical length range of 20-70 mm [6]. The mixed compounds are then directly put in the mold to be compression molded. The flow effect, which is dependent on the charge placement and the part geometry during compression molding, leads to the partial alignment of fibers.

Composites are particularly strong in the direction of fiber alignment. Hence, it is important to study the dynamics of fiber orientation in composite manufacturing process. Fiber orientation models originate from Jeffrey's model[7] which describes ellipsoids behaviour under Stokes drag[8]:

$$\frac{dp}{dt} = \omega \cdot p + \lambda(D \cdot p - (p^T \cdot D \cdot p)p)$$

Where ω is a vorticity tensor, D is the deformation tensor and λ is a function of axis ratio l/d.

$$\omega = 0.5(L - L^T)$$

$$D = 0.5(L + L^T)$$

$$L = \begin{pmatrix} \frac{dv_x}{dx} & \frac{dv_y}{dy} & \frac{dv_z}{dz} \\ \frac{dv_x}{dy} & \frac{dv_y}{dy} & \frac{dv_z}{dy} \\ \frac{dv_x}{dz} & \frac{dv_y}{dz} & \frac{dv_z}{dz} \end{pmatrix}$$

$$\lambda = \frac{l/d^2 - 1}{l/d^2 + 1}$$

Although validated multiple times in experimental works[9-14], Jeffery's model is only applicable for short fibers in diluted systems. In order to apply Jeffery's model to composites Folgar and

Tucker [15] have modified Jeffery's model to account for interaction between fibers thus allowing it to be used in concentrated fiber system. Later Advani and Tucker[16] rewrote the model to its current form by defining orientation tensor a, thus calculating overall fiber orientation at a certain location instead of calculating the orientation of each fiber.

$$\frac{da}{dt} = (\omega \cdot a - a \cdot \omega) + \lambda(D \cdot a + a \cdot D - 2a_4 : D) + 2dC_I\dot{\gamma}(\frac{I}{d} - a)$$

$$a = \int p \otimes p \, \psi(p) dp$$

Where C_I is an empirical interaction coefficient, a_4 is 4th order orientation tensor, I is identity matrix and $\psi(p)$ is orientation distribution density function. The term $2dC_I\dot{\gamma}(\frac{I}{d} - a)$ is referred to as Isotropic Rotary Diffusion term A^{IRD}. The fourth order orientation tensor a_4 can be approximated through second order orientation tensor *a* using the "quadratic approximation"[17, 18]: $a \otimes a = a_4$

Although Folgar and Tucker adapted Jeffery's model to concentrated solutions, their model could still only handle short fibers. The Anisotropic Rotary Diffusion model (ARD) [19] was specifically designed for longer fibers. In this model, the Folgar-Tucker isotropic rotary diffusion term A^{IRD} is replaced for anisotropic rotary diffusion term A^{ARD}:

$$A^{ARD} = \dot{\gamma}[2C - 2(tr\ C)a - 5(C \cdot a + a \cdot C) + 10a_4 : C]$$

Where, C is rotary diffusion tensor defined as: $C = b_1 I + b_2 a + b_3 a^2 + b_4 \frac{D}{\dot{\gamma}} + b_5 \frac{D^2}{\dot{\gamma}^2}$,

with b_i being empirical constants.

Huan-Chang Tseng et. al have improved the model further by introducing improved Anisotropic Rotary Diffusion (iARD) made by combining Folgar-Tucker Isotropic Rotary Diffusion term with Fiber Rotary Resistance term thus yielding a model which has only two parameters C_I, C_M instead of the original five and combined it with Retarding Principle Rate (RPR) model with one parameter thus accounting for fiber-matrix interactions[20]:

$$A^{iARD+PRP} = A^{iARD} + A^{PRP}$$

$$A^{iARD} = A^{IRD} + A^{FRR}$$

$$A^{FRR} = 2\dot{\gamma}C_I C_M \left\{(a - \hat{L}) + 5[0.5(a \cdot \hat{L}) + 0.5(a \cdot \hat{L})^T - a_4 : \hat{L}]\right\}$$

Where, $\hat{L}$ is dimensionless fiber-rotary-resistance tensor defined as: $\hat{L} = \frac{L^T \cdot L}{L^T : L}$

$$A^{PRP} = -R \cdot \Lambda^{IOK} \cdot R^T$$

Where $R = [e_1, e_2, e_3]$ is rotation matrix defined by three eigenvector columns of a and Λ^{IOK} is a material derivative of a diagonal matrix.

Λ^{IOK} three components are given by:

$$\Lambda_{ii}{}^{IOK} = \alpha[\lambda_i - \beta(\lambda_i^2 + 2\lambda_j\lambda_k)]$$

Where α, β are constants.

iARD-PRP model is implemented in Moldex3D for fiber orientation calculation. For composites with partly aligned and discontinuous fibers, several approaches are available to predict Young's modulus. The modified rule of mixture (MROM) is the most widely used one, which is based on the shear lag model developed by Cox [21] and improved by Krenchel [22]. The empirical Halpin-Tsai model [23, 24] has also proved to work well with the prediction of Young's modulus of discontinuous fiber reinforced composites. Another approach is based on laminate analogy approach (LAA) with an assumption that the specimen is shell-like to enable the condition of a planar fiber orientation distribution (FOD) [25]. This work performs a comparison between the predicted Young's modulus with two existing models and the experimental result.

2 Experimental

2.1 Materials and Preparation

PA6 (Ultramid® 8202HS) provided by BASF and glass fiber (StarRov 886) provided by Johns Manville were used in this work. Preparation was performed on Dieffenbacher direct long fiber reinforced thermoplastics in-line compounding D-LFT line at the Fraunhofer Project Center for Composites Research (FPC@Western). The schematic of the line is shown in **Figure 1**. During

processing, PA6 granules were dried and fed into the first extruder to undergo a thorough melting. Then the molten matrix was extruded out through a film die into the second extruder for compounding. Simultaneously, continuous glass fibers were integrated from the top of the melt film and continuously pulled into the second extruder by the screw rotation. In the second extruder, the continuous fibers were chopped by a specially designed cutting element of the twin-screw and smoothly dispersed by shear effect of the melt. Mixed compounds continuously come out through a servo die and are cut into charges by a shear blade. The charges were kept warm on an insulated conveyor and transferred manually into a tool to undergo compression molding. Flat plaques were manufactured, with a size of 457×457×3 mm^3. The charge with a size of 350×100×30 mm^3 was placed on one edge of the mold to increase the flow distance. The fiber content for this plaque was set to be 30wt%.

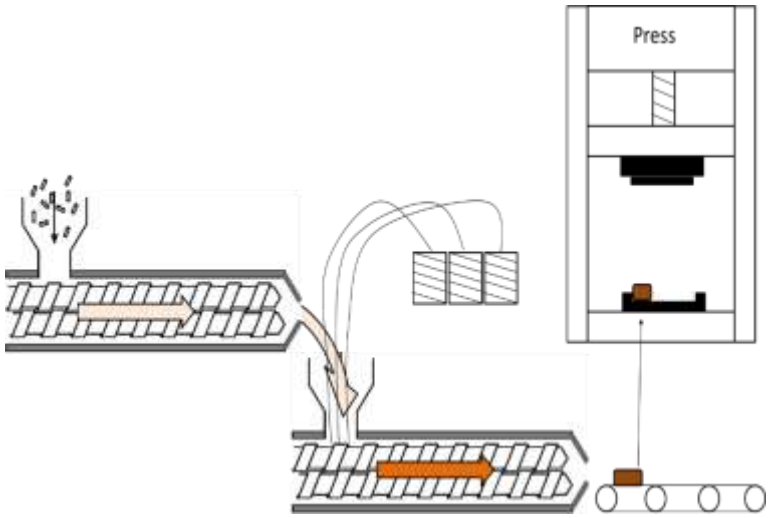

Figure 1: *Schematic of Dieffenbacher D-LFT-ILC line*

2.2 Moldex3D simulation

Pure triangle mesh was created in Rhinoceros 5 as shown in **Figure 2** and its parameters are summarised in **Table 1**.

Table 1: *Solid mesh characteristics*

Dimensions	457x457x3 mm
Layers in cavity mesh	10
Layers in compression zone mesh	30
Charge dimensions	457x94.4x17.7 mm

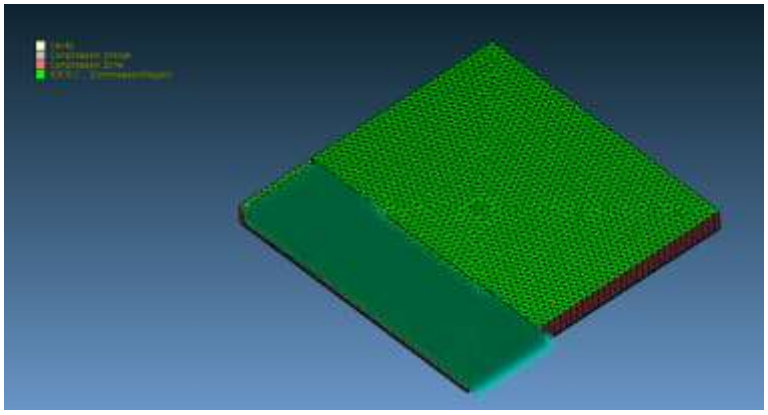

Figure 2: *Plaque mesh*

BASF Nypel 6030G HS-BK was selected from the Moldex3D material data bank; where aspect ratio was changed to 600 from the original 20. Velocity of the upper plate was set to 10 mm/sec and for long fibers in Moldex3D iARD fiber orientation model was selected, model parameters are summarised in **Table 2**.

Table 2: *iARD model parameters*

C_i	0.01
C_m	1
RPR alpha factor	0.1

As the initial fiber orientation in the charge is unknown, two opposite extreme cases were studied in the simulation. Initial conditions of case A are shown in **Figure 3 (a)**, with all the fibers oriented in the direction of the charge. Initial conditions of case B are shown in **Figure 3 (b)** with all the fibers initially perpendicular to the charge direction.

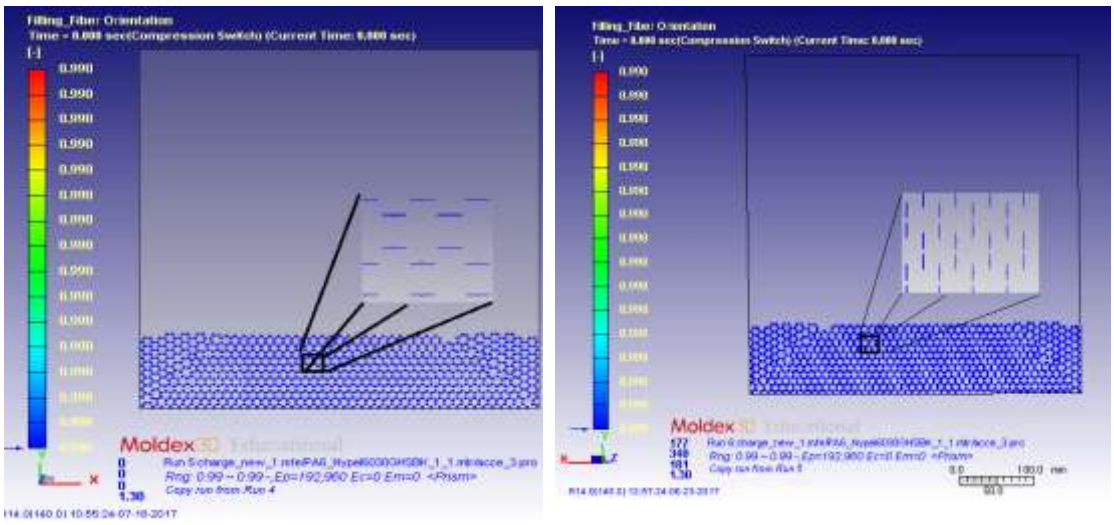

(a) **(b)**

Figure 3: *Fiber orientation initial condition for: (a) case A, all the fibers are oriented in the direction of the charge and (b) case B, all the fibers are perpendicular to the charge*

2.3 Tensile test

Tensile tests were performed on an Instron 8804 load frame with a 250 kN load cell based on ASTM standard. All samples were dried in a vacuum assisted oven at 100°C for 48 hours prior to the tests. The crosshead speed was 2 mm/min. An extensometer with a gauge length of 50 mm was used to measure the strain.

2.4 Measurement of fiber length and orientation

The measurement of fiber length distribution was performed at the University of Wisconsin-Madison. Firstly, the examined samples were burned to eliminate the matrix. Then the residual samples were dispersed in water and placed on a flat surface. They were scanned and analyzed by a software with a special algorithm [26] to identify the individual fibers and to get the fiber length distribution.

Fiber orientation was measured in two steps. Firstly, a $9\times3\times1mm^3$ sample cut from the plaque as shown in **Figure 4** was scanned using a GE eXplore SP "MS" Micro-CT, with 6-micrometer resolution to get 3D images of the specimen. The 3D images were viewed section by section through thickness and transmitted as 2D images of the cross section. Then all the 2D images were analyzed quantitatively with Orientation J software package to obtain the fiber orientation distribution through the thickness.

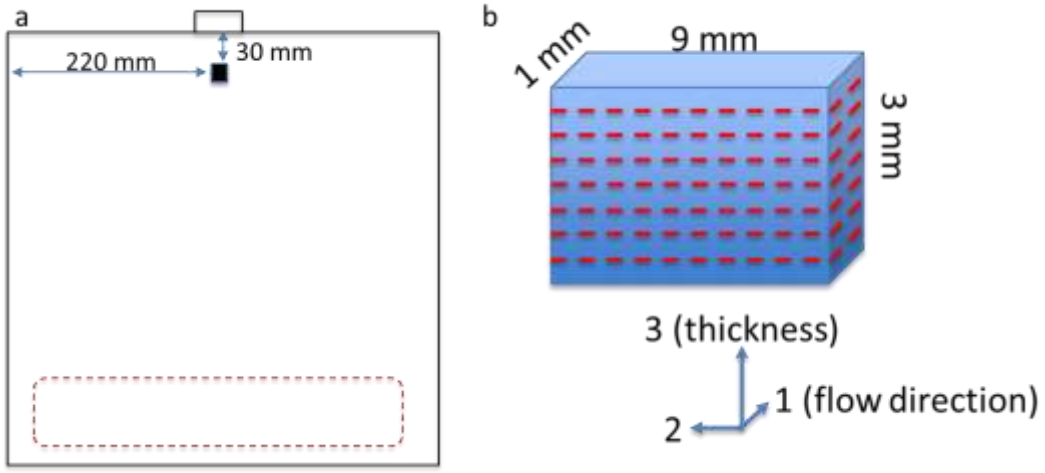

Figure 4: *Schematic showing a) Position and b) size of the sample cut for micro-CT scan*

2.5 Prediction of mechanical properties

Modified rule of mixture

Based on rule of mixture (ROM), modified rule of mixture (MROM) uses two factors, k_1 and k_2, to take the fiber length distribution (FLD) and fiber orientation distribution (FOD) into account, respectively. The expressions are shown below:

$$E_{11} = k_1 k_2 E_f V_f + E_m(1 - V_f)$$

$$\text{with } k_1 = [1 - \frac{\tanh\left(\frac{\beta L}{2}\right)}{\frac{\beta L}{2}}]$$

$$\beta = \frac{2}{d}[\frac{2G_m}{E_f \ln\sqrt{\frac{\pi}{X_i V_f}}}]$$

$$k_2 = \sum_i a_i \cos^4\theta_i$$

Where E_f and E_m are the Young's moduli of fibers and matrix, respectively. The effects of FLD and FOD were incorporated through the fiber length factor k_1 and fiber orientation factor k_2. L

and d are the length and diameter of fibers, respectively. X_i depends on the geometrical packing arrangement of fibers and can be set as 4. V_f is fiber volume fraction. a_i represents the fiber proportion making an angle θ_i with the load direction [27].

Halpin-Tsai model

The first step only takes the fiber length distribution (FLD) into account. The longitudinal E_{UD1} and transverse E_{UD2} Young's modulus of unidirectional discontinuous fiber reinforced counterpart is predicted at first with the expressions shown below [28]:

$$E_{udi} = E_m \cdot \left(\frac{1 + \zeta_i \eta_i V_f}{1 - \eta_i V_f} \right)$$

$$With\ \eta_i = \left(\frac{\frac{E_f}{E_m} - 1}{\frac{E_f}{E_m} + \zeta} \right)$$

Where ζ_1=2L/d andζ_2=2, E_m is the Young's modulus of matrix, V_f is the fiber volume fraction. L is the fiber length and d is the fiber diameter. Then the fiber orientation distribution (FOD) is taken into account with the expressions shown below:

$$E_c = k_2 E_{UD1} + E_{UD2}(1 - k_2)$$

3. Result and analysis

3.1 Fiber orientation predicted by Moldex3D simulation

Mold filling results are presented in **Figure 5**. It could be seen from the flow front that the flow is almost uniform in the *y* direction. **Figure 6 (a)** presents the fiber orientation on the skin for case A. Although the initial orientation starts perpendicular to the direction of the flow, by the middle of the plaque most of the fibers are oriented in the direction of the flow. Toward the end of the flow path, the fibers are no longer oriented in the direction of the flow due to the wall effect and approach random orientation. The orientation in the middle of the thickness of the panel (middle of z axis from Figure 4) for case A is presented in **Figure 6 (b)**. The middle of panel orientation differs from the skin orientation. The fibers in the middle of the panel are less oriented in the flow direction than the fibers in the skin. This could be explained by freezing of the material near the mold surface thus preventing the future changes in the fiber orientation. **Figure 7 (a)** shows

the skin orientation for case B. Without walls it would be expected for the orientation not to change as it is already in the direction of the flow; however, it could be seen that the orientation is changing from highly oriented fibers in the direction of the flow toward more random oriented fibers. **Figure 7 (b)** shows that the fibers in the middle of the thickness of the panel are less oriented than on the skin for Case B.

Fiber orientation tensor was calculated at the location where specimen was taken. Tensor orientation values, shown in **Table 3**, of term A_{zz}, A_{xz} and A_{yz} are close to zero which indicates that the fibers in the plaque have a planar orientation. For case A, the value of A_{yy} decreases from both surfaces to the core which indicates that fibers at the core are less aligned in flow direction than those at the surfaces. For case B, three peaks of A_{yy} at the two surface and the core indicate that the initial in-flow fiber alignment (perpendicular to the direction of the charge) can result in more fibers at the core aligned in the flow direction.

Table 3: *Fiber orientation tensor at selected location shown at* ***Figure 5***

Case	z location (height)	Axx	Ayy	Azz	Axy	Axz	Ayz
Case A	0						
	0.15	0.269	0.730	0.001	-0.002	0.000	0.012
	0.45	0.337	0.662	0.001	-0.003	0.000	0.004
	0.75	0.345	0.655	0.001	-0.003	0.000	0.005
	1.05	0.350	0.649	0.001	-0.003	0.000	0.005
	1.35	0.384	0.614	0.002	-0.003	0.000	0.003
	1.65	0.400	0.598	0.002	-0.004	0.000	-0.002
	1.95	0.337	0.662	0.001	-0.003	0.000	-0.007
	2.25	0.313	0.686	0.001	-0.003	0.000	-0.006
	2.55	0.300	0.699	0.001	-0.004	0.000	-0.008
	2.85	0.281	0.713	0.005	-0.002	0.000	-0.018
Case B	0						
	0.15	0.255	0.743	0.002	-0.002	0.000	0.014
	0.45	0.336	0.663	0.001	-0.003	0.000	0.004
	0.75	0.340	0.659	0.001	-0.003	0.000	0.005
	1.05	0.332	0.666	0.002	-0.002	0.000	0.005
	1.35	0.281	0.717	0.003	-0.001	0.000	0.000
	1.65	0.226	0.771	0.003	-0.001	0.000	0.000
	1.95	0.281	0.717	0.003	-0.002	0.000	-0.004
	2.25	0.302	0.696	0.002	-0.003	0.000	-0.006
	2.55	0.291	0.707	0.002	-0.004	0.000	-0.009
	2.85	0.264	0.729	0.007	-0.002	0.000	-0.020

The fiber orientation factors can be calculated based on the equation below:

$$k_2 = \sum_i a_i \cos^4 \theta_i$$

The average fiber orientation factor k_2 was calculated to be 0.67 for Case A, 0.71 for Case B.

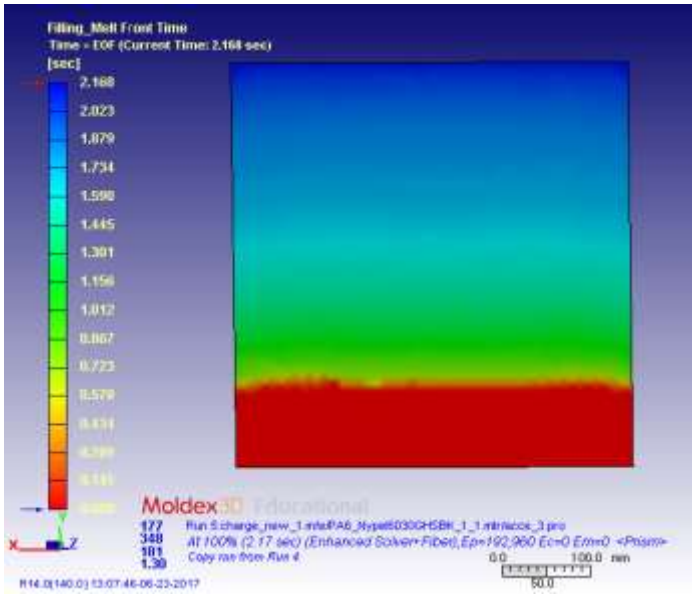

Figure 5: *Mold filling behaviour*

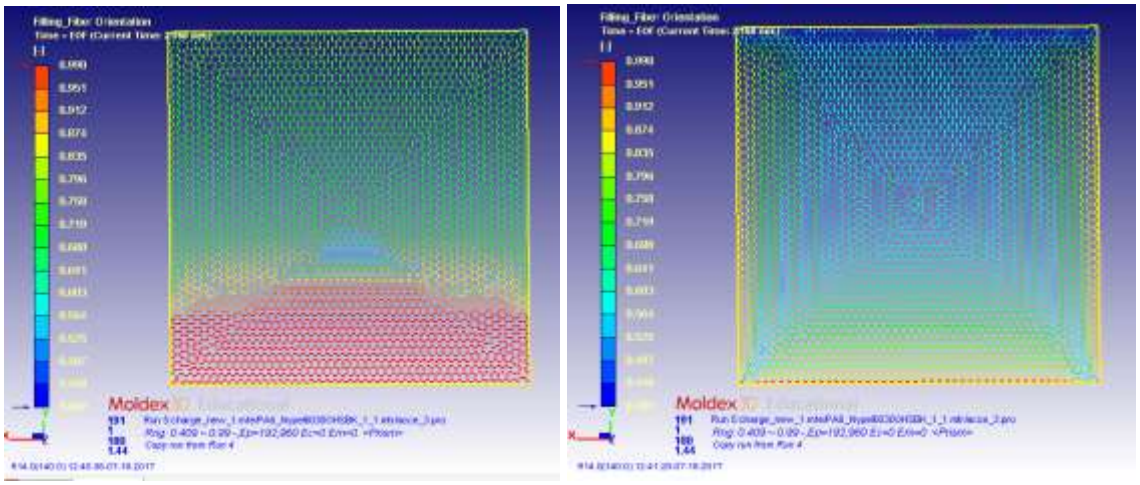

(a) (b)

Figure 6: *Fiber orientation in case A: (a) skin (0.02 mm from the lower mold surface) (b) middle*

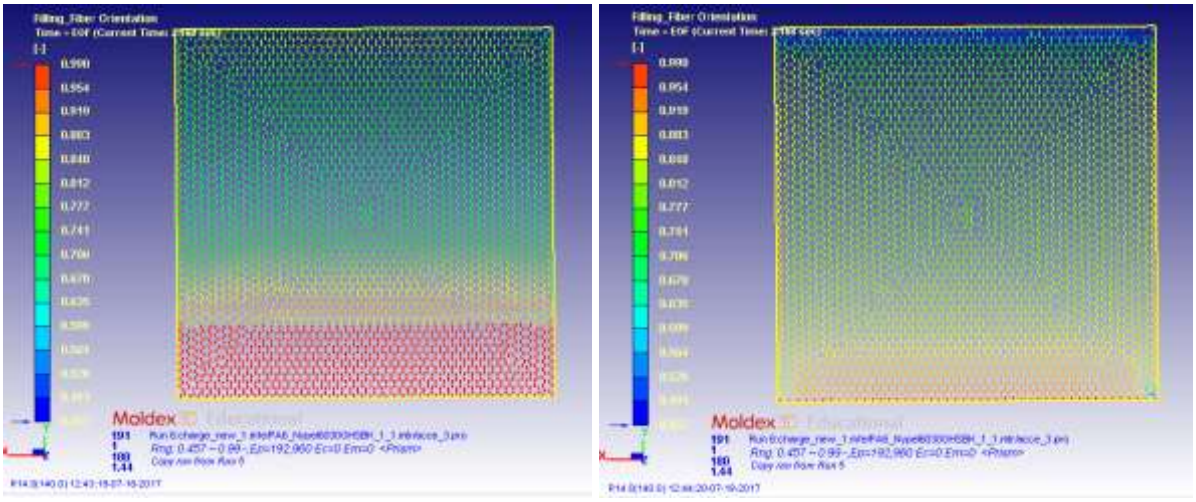

(a) (b)

Figure 7: *Fiber orientation in case B: (a) skin (0.02 mm from the lower mold surface) (b) middle*

3.2. Fiber orientation distribution characterized by Micro-CT

The Micro-CT images in **Figure 9** show the fibers distributed in the matrix. The analysis was done on 9 sections through thickness with the distance between two sections of 0.36mm. The sections are at three different positions in the specimens, as labelled top, center and bottom, respectively. The fiber orientation distribution (FOD) of each section was calculated using Orientation J and shown in **Figure 10**. The global FOD function is derived as $a_i = 0.05e^{-0.05\theta_i}$, where a_i is the portion of fibers aligned in θ_i degree. The average fiber orientation factor k_2 was calculated to be 0.75.

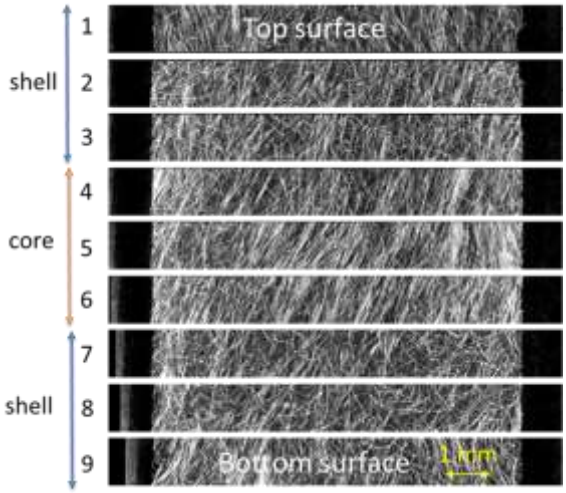

Figure 8: *Images of through- thickness cross sections by micro-CT scan at 6μm resolution*

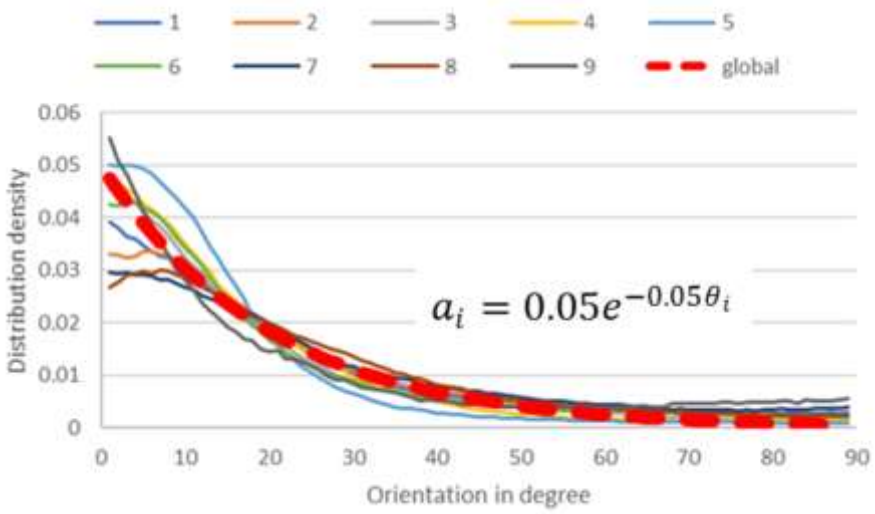

Figure 9: *Fiber orientation distribution (FOD) measured on nine layers of a D-LFT sample as shown in* ***Figure*** *8*

3.3. Fiber length distribution observed by Micro-CT

The fiber length distribution (FLD) of a 100mm×100mm square sample cut from the same plaque are shown in **Figure 10**. The numerical average fiber length (L_n) and length weighted average fiber length (L_l) are calculated to be 3.93 mm and 8.77 mm, respectively. The existence of a large amount of short fibers (<300 micrometers) results in the difference which can be related to the fiber attrition during the extrusion process. In addition, the operation of fibers dispersion during the fiber length measurement might caused some damage to the fibers due to the massive fiber entanglements.

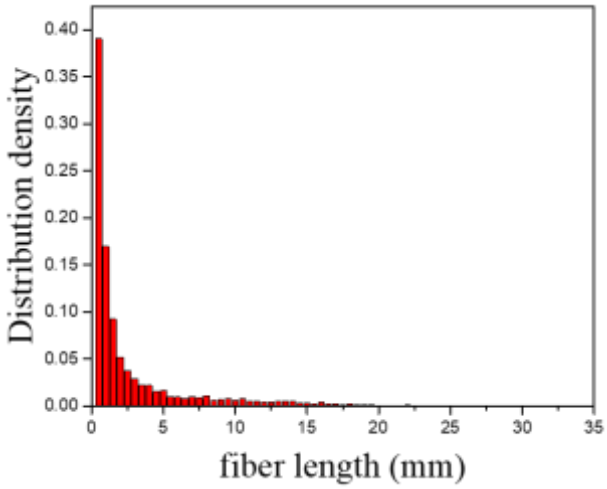

Figure 10: *Measured fiber length distribution (FLD) of D-LFT with 30wt% fiber*

3.4. Prediction of mechanical properties

Based on the following equations, the fiber length factor, k_1 is calculated to be 0.99 if L_l is taken as 8.77 mm.

$$k_1 = [1 - \frac{\tanh\left(\frac{\beta L}{2}\right)}{\frac{\beta L}{2}}]$$

$$\beta = \frac{2}{d}[\frac{2G_m}{E_f \ln\sqrt{\frac{\pi}{X_i V_f}}}]^{1/2}$$

With the calculated k_1 and k_2, the Young's modulus was predicted by two models and compared with the experimental results, as shown in **Figure 11**. In case A, the Young's modulus was predicted to be 10.05 GPa with the MROM model and 10.61 GPa with the H-T model, in which the latter is closer to the experimental result. In case B, the Young's modulus was predicted to be 10.51 GPa with the MROM model and 10.99 GPa with the H-T model, in which the former is closer to the experimental result. Since the sample for micro-CT scan is very small (9×3×1 mm^3), the poorer prediction from the micro-CT might be related to the spatial variation of fiber distribution within the D-LFT plaque.

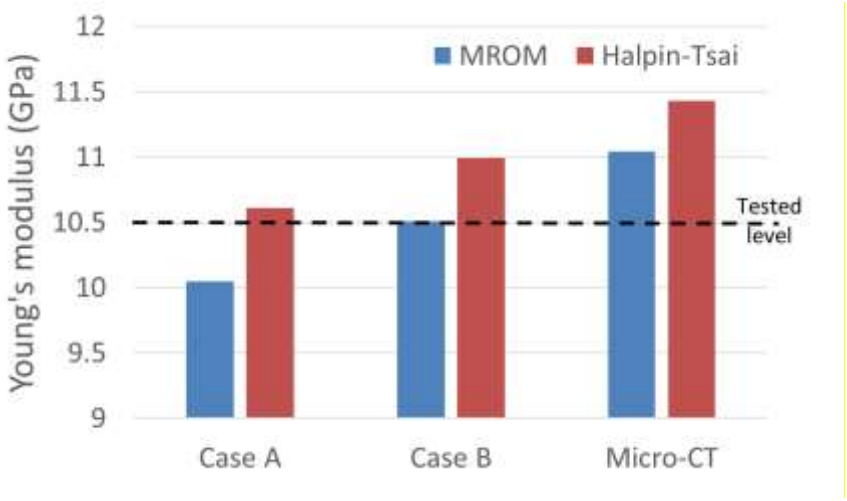

Figure 11: *Predicted Young's modulus by both MROM and Halpin-Tsai model using fiber orientation factor derived from Case A and Case B of Moldex3D simulation and Micro-CT scan*

4. Conclusion

Fiber orientation in long glass fiber reinforced polyamide 6 D-LFT composite was predicted using Moldflow3D simulation and compared with experimental characterization using micro-CT method. The core and skin showed varied fiber orientation. Halpin-Tsai and MROM models were used to predict the mechanical properties of the system by incorporating fiber length and orientation factors. The predicted Young's modulus was consistent with experimental results. It was indicated that an ICME model has valuable potential for the D-LFT process.

5. Acknowledgement

The present research was supported by the Natural Sciences and Engineering Research Council of Canada *(*NSERC*)* through the Automotive Partnership Canada (APC) program and industrial support from General Motors of Canada Ltd. (GMCL), BASF, Johns Manville (JM), Dieffenbacher North America (DNA) and Elring-Klinger. The authors would like to thank Louis Kaptur from DNA and all those at the Fraunhofer Project Center for their efforts in manufacturing the materials examined in this study.

Reference:

[1] F. Henning, W. Krause, H. Ernst, and R. Brussel, LFT-D-ILC-Innovative Process Technology Decreases the Costs of Large-Scale Production of Long-Fiber-Reinforced Thermoplastic Components (1124). In *ANTEC-CONFERENCE PROCEEDINGS*- Vol. 3, pp. 2558-2562, 2002

[2] F. Henning, H. Ernst and R. Brüssel, LFTs for automotive applications. *Reinforced plastics*, Vol. 49, no. 2, pp. 24-33, 2005.

[3] S. Y. Fu, X. Hu, C. Y. Yue, Effects of fiber length and orientation distributions on the mechanical properties of short-fiber-reinforced polymers. *Journal of the Society of Materials Science, Japan*, vol. 48*,* pp. 74-83, 1999.

[4] S. Mortazavian, and A. Fatemi, Effects of fiber orientation and anisotropy on tensile strength and elastic modulus of short fiber reinforced polymer composites. *Composites Part B: Engineering*, vol. 72, pp. 116-129, 2015.

[5] J. Hohe, C. Beckmann and H. Paul, Modeling of uncertainties in long fiber reinforced thermoplastics. *Materials & Design*, vol. 66, pp. 390-399, 2015.

[6] W. Krause, F. Henning, S. Tröster, O. Geiger and P. Eyerer, LFT-D - a process technology for large scale production of fiber reinforced thermoplastic components. *Journal of Thermoplastic Composite Materials*, vol. 16, no. 4, pp. 289-302, 2003.

[7] G. B. Jeffery, “The Motion of Ellipsoidal Particles Immersed in a Viscous Fluid,” *Proc. R. Soc. A Math. Phys. Eng. Sci.*, vol. 102, no. 715, pp. 161–179, 1922.

[8] G. Youngren and A. Acrivos, “Stokes flow past a particle of arbitrary shape: a numerical method of solution,” *J. Fluid Mech.*, vol. 69, no. 2, pp. 377–403, 1975.

[9] G. I. Taylor, “The Motion of Ellipsotdal Parttcles in ct Viscous Fluid .,” *Proc. R. Soc. London. Ser. A, Contain. Pap. a Math. Phys. Character*, vol. 103, no. 720, pp. 58–61, 1923.

[10] B. . Trevelyan and S. . Mason, “Particle motions in sheared suspensions. I. Rotations,” *J. Colloid Sci.*, vol. 6, no. 4, pp. 354–367, 1951.

[11] S. G. Mason and R. S. J. Manley, “Particle Motions in Sheared Suspensions: Orientations and Interactions of Rigid Rods,” *Proc. R. Soc. A Math. Phys. Eng. Sci.*, vol. 238, no. 1212, pp. 117–131, 1956.

[12] E. Anczurowski, “Particle Motions in Sheared Suspensions. XXIV. Rotation of Rigid Spheroids and Cylinders,” *J. Rheol. (N. Y. N. Y).*, vol. 12, no. 2, pp. 209, 1968.

[13] E. Anczurowski, R. G. Cox, and S. . Mason, “The kinetics of flowing dispersions IV. Transient orientations of cylinders,” *J. Colloid Interface Sci.*, vol. 23, no. 4, pp. 547–562, 1967.

[14] E. Anczurowski and S. Mason, “The kinetics of flowing dispersions : III. Equilibrium orientations of rods and discs (experimental),” *J. Colloid Interface Sci.*, vol. 23, no. 4, pp. 533–546, 1967.

[15] F. Folgar and C. L. Tucker, “Orientation Behavior of Fibers in Concentrated Suspensions,” *J. Reinf. Plast. Compos.*, vol. 3, no. 2, pp. 98–119, 1984.

[16] S. G. Advani and C. L. Tucker, “The Use of Tensors to Describe and Predict Fiber Orientation in Short Fiber Composites,” *J. Rheol. (N. Y. N. Y).*, vol. 31, no. 8, p. 751, 1987.

[17] E. J. Hinch and L. G. Leal, “Constitutive equations in suspension mechanics. Part 2. Approximate forms for a suspension of rigid particles affected by Brownian rotations,” *J. Fluid Mech.*, vol. 76, no. 01, p. 187, 1976.

[18] G. G. Lipscomb, M. M. Denn, D. U. Hur, and D. V. Boger, “The flow of fiber suspensions in complex geometries,” *J. Nonnewton. Fluid Mech.*, vol. 26, no. 3, pp. 297–325, 1988.

[19] J. H. Phelps and C. L. Tucker, “An anisotropic rotary diffusion model for fiber orientation in short- and long-fiber thermoplastics,” *J. Nonnewton. Fluid Mech.*, vol.156, pp. 165-176, 2009.

[20] H.-C. Tseng, R.-Y. Chang, and C.-H. Hsu, “Phenomenological improvements to predictive models of fiber orientation in concentrated suspensions,” *J. Rheol. (N. Y. N. Y).*, vol. 57, no. 6, pp. 1597, 2013.

[21] H. L. Cox, The elasticity and strength of paper and other fibrous materials. *British journal of applied physics*, vol. 3*, no.* 3, pp. 72, 1952.

[22] H. Krenchel. Fibre reinforcement; theoretical and practical investigations of the elasticity and strength of fibre-reinforced materials. Akademisk Forlag. *Copenhagen, Denmark*, 1964.

[23] J. C. Affdl, & J. L. Kardos, The Halpin-Tsai equations: a review. *Polymer Engineering & Science*, vol. 16, no. 5, pp. 344-352, 1976.

[24] J. L. Thomason, The influence of fibre length and concentration on the properties of glass fibre reinforced polypropylene. 6. The properties of injection moulded long fibre PP at high fibre content. *Composites Part A: Appl. S. vol.* 36, no. 7, pp. 995-1003, 2005.

[25] S. Y. Fu and B. Lauke, The elastic modulus of misaligned short-fiber-reinforced polymers. *Composites science and technology*, vol. 58, no. 3-4, pp. 389-400, 1998.

[26] V. Kunc, B. J. Frame, B. N. Nguyen, C. L. Tucker III and G. Velez-Garcia, Fiber length distribution measurement for long glass and carbon fiber reinforced injection molded thermoplastics. *Research Gate*, 2007.

[27] E. Lafranche, V. M. Oliveira, C. I. Martins and P. Krawczak, Prediction of injection-moulded flax fibre reinforced polypropylene tensile properties through a micro-morphology analysis. *Journal of Composite Materials*, vol. 49, no. 1, pp. 113-128, 2015.

[28] J. C. Affdl and J. L. Kardos, The Halpin-Tsai equations: a review. *Polymer Engineering & Science*, vol. 16, no. 5, pp. 344-352, 1976.